Linear optical model for a large ground based telescope

George Z. Angeli[1] and Brooke Gregory[2]

[1]New Initiatives Office, AURA Inc.
[2]Cerro Tololo Inter-American Observatory, NOAO

ABSTRACT

A linear optical model for 30 m class astronomical telescopes is discussed. Our approach to modeling the optical performance of the telescope is an extension of the line-of-sight analysis to incorporate low order image aberrations. The model describes the optical path difference at the telescope exit pupil as a linear combination of primary and secondary mirror displacements and deformations in a Zernike basis. Although the model is valid over a significant, useful range of deformation amplitude and field of view, it is particularly convenient for the design and investigation of active optics control systems operating close to the desired condition of an unperturbed telescope. The formalism of the linear model and comparison with the OPD results generated by ray-tracing are discussed.

Keywords: active optics, linear optical model, telescope control, Extremely Large Telescopes, optical aberration, Zernike decomposition

1 INTRODUCTION

The stability and control of 30 m class astronomical telescopes, like the Giant Segmented Mirror Telescope (GSMT) [1] require active control of the telescope mirrors. Wind, thermal and gravitational forces introduce large amplitude, low spatial-frequency distortions into the structure and hence the optical surfaces. Due to the limited dynamic range of adaptive optics systems, a layered control approach is required to achieve the desired performance. As part of this layered approach, wavefront sensor based active optics control of the mirrors is usually necessary.

The structural dynamics of the telescope can be approximated, with reasonable fidelity, by linear, time invariant differential operators, assuming proportional damping and negligible hysteresis [2]. The parameters of these operators are usually derived from finite element analysis or direct measurements [3]. Similarly, by neglecting actuator and sensor nonlinearities, the control laws are typically linear, time invariant differential operators. A linear optical model of the telescope would enable us to take advantage of the well-developed tools of linear system theory in the design and analysis of the optical feedback loops.

The traditional way to characterize the dynamic performance of an astronomical telescope is the separate estimate of image jitter (line-of-sight analysis) and image aberration. However, the jitter can be expressed in terms of the back focal length and exit pupil wavefront tilt, which in turn is associated with Zernike aberration terms #1 and #2 [4] (see Appendix for Zernike terms used in this paper). This provides an opportunity for uniform treatment of jitter and image aberration.

The OPD $\boldsymbol{\varepsilon}$, for a particular field point, measured at the exit pupil, is a good measure of the telescope performance because the major characteristics of image quality – like the point spread function, Strehl ratio or encircled energy – can be directly derived from it. We take the OPD, then, as the output of the telescope optical system. A perfect telescope would produce a converging, spherical wavefront at the exit pupil of the system, with the nominal focus at the center of the sphere. The actual wavefront can be constructed to coincide with the ideal one at point "O", the

gangeli@noao.edu AURA New Initiatives Office, 950 N. Cherry Ave. Tucson, AZ 85719
bgregory@ctio.noao.edu Cerro Tololo Inter-American Observatory, NOAO, Casilla 603, La Serena, Chile

center of the pupil (see Figure 1). In the ray tracing approximation, the OPD is defined to be the signed displacement of the output wavefront in the +z direction, at point P, measured from the spherical wavefront along the ray direction [4]. Thus, for example, a positive OPD occurs when the wave-field lags behind the reference sphere, as in Figure 1 at point P. We have adopted the convention that the +z direction points from the primary mirror to the secondary one, in the optical axis of the telescope.

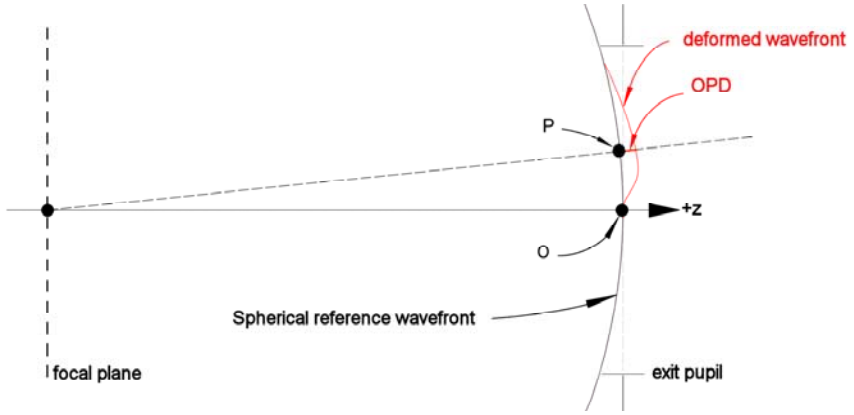

Figure 1 Exit pupil OPD definition and sign convention

For an on-axis object, the center of the exit pupil reference sphere, i.e. the nominal focus, is also on axis. For off-axis objects, like guide stars, the center of the reference sphere is no longer on the optical axis, but its position can nonetheless be unambiguously defined.

The inputs of the optical system are the deformations and displacements of the optical surfaces, which can be related directly to the nodal displacements **q** in the structure. A linear model of the optical response of the telescope is created by introducing a sensitivity (Jacobian) matrix **S**, which is defined in Equations (1.1) and (1.2). Another way of looking at Equation (1.2) is that the linear optical response of the system is approximated by the local slope of the nonlinear response curves at a given operating point [5]. The operating point is $\boldsymbol{\varepsilon} = \boldsymbol{\varepsilon}_{tel}$ @ $\mathbf{q} = \mathbf{0}$ which is a constant offset containing the possible intrinsic aberrations of the telescope.

$$\boldsymbol{\varepsilon} = \boldsymbol{\varepsilon}_{tel} + \mathbf{S}\mathbf{q} + (\text{higher order terms}) \tag{1.1}$$

$$\mathbf{S} = \begin{bmatrix} \left(\frac{\partial \varepsilon_1}{\partial q_1}\right)_{q_1=0} & \cdots & \left(\frac{\partial \varepsilon_1}{\partial q_m}\right)_{q_m=0} \\ \vdots & \left(\frac{\partial \varepsilon_i}{\partial q_k}\right)_{q_k=0} & \vdots \\ \left(\frac{\partial \varepsilon_n}{\partial q_1}\right)_{q_1=0} & \cdots & \left(\frac{\partial \varepsilon_n}{\partial q_m}\right)_{q_m=0} \end{bmatrix} \tag{1.2}$$

Here the possible **q** vectors define a space $\mathfrak{Q}$, which is linear. It is worth noting that $\mathfrak{Q}$ is also a normed space with a scalar (inner) product defined as the RMS deformation; hence it is a Hilbert space.

Usually a significant number of columns in **S** contain only zero elements corresponding to nodes with no influence on the optical response. These columns can be removed from the sensitivity matrix, expediting further calculations. However, for a system as large as a 30 meter class astronomical telescope, even the truncated **S** matrix is prohibitively large. There are cases of system analysis, where it is necessary to keep all the information embedded in

the sensitivity matrix in order to get meaningful results. A good example is an uncontrolled segmented mirror exposed to direct wind pressure with short correlation length, where the segments are responding by and large independently.

On the other hand, many problems don't require full knowledge of **S**. Characteristic examples are: secondary mirror rigid body control, and active optical control of a – segmented or monolithic – primary mirror [6]. In the case of a segmented primary mirror, although mechanical feedback loops can take care of the higher order deformations and preserve continuity of the mirror, lower order mirror deformations are sensed rather poorly by edge sensors [7,8]. Unfortunately, the sensitivity matrix, as defined in Equation (1.2) in terms of structural node displacements, cannot be partitioned into "low order" and "higher order" mirror deformations without further modification

In Section 2, we suggest a way to partition the sensitivity matrix and then relate these partitions to the shape and displacement of the primary and secondary mirrors.

2 LINEAR OPTICAL MODEL BASED ON ZERNIKE BASIS SETS

The linearly independent set of structural modes, $\mathbf{q_m}$, generates a linear manifold $\mathcal{M}$ in space $\mathcal{Q}$. In other words, all possible values of $\mathbf{q}$ are linear combinations of $\mathbf{q_m}$.

$$\mathbf{q} = \mathbf{\Phi q}_m \tag{2.1}$$

Operator $\mathbf{\Phi}$ is the eigenvector matrix of $\mathcal{M}$ containing the modes as columns, while in the vector $\mathbf{q}_m$ are the coefficients defining the modal coordinates.

$$\boldsymbol{\varepsilon} \approx \boldsymbol{\varepsilon}_{tel} + \mathbf{Sq} = \boldsymbol{\varepsilon}_{tel} + \mathbf{S\Phi q}_m \tag{2.2}$$

A convenient way to describe the telescope structure is its modal state representation [2,9]. Since the states are directly related to the modal coordinates ($\mathbf{x} = \begin{bmatrix} \mathbf{q}_m^{\mathrm{T}} & \dot{\mathbf{q}}_m^{\mathrm{T}} \end{bmatrix}^{\mathrm{T}}$), the optical output matrix for exit pupil OPD is straightforward.

$$\mathbf{C} = \mathbf{S\Phi}\begin{bmatrix} \mathbf{I} & \mathbf{0} \end{bmatrix} \tag{2.3}$$

Let us now partition $\mathcal{M}$ into subspaces according to the optical surfaces, i.e. the primary and secondary mirrors. When $\mathcal{M}$ contains only the degrees of freedom affecting the optical response, that is, when **S** is truncated, these subspaces are orthogonal complements of each other.

$$\begin{aligned} \mathbf{q} &= \begin{bmatrix} \mathbf{q}_p \\ \mathbf{q}_s \end{bmatrix} \\ \mathbf{\Phi} &= \begin{bmatrix} \mathbf{\Phi}_p \\ \mathbf{\Phi}_s \end{bmatrix} \\ \mathbf{S} &= \begin{bmatrix} \mathbf{S}_p & \mathbf{S}_s \end{bmatrix} \end{aligned} \tag{2.4}$$

The linear approximation of Equation (1.1) becomes

$$\boldsymbol{\varepsilon} \approx \boldsymbol{\varepsilon}_{tel} + \mathbf{S}_p\mathbf{\Phi}_p\mathbf{q}_m + \mathbf{S}_s\mathbf{\Phi}_s\mathbf{q}_m = \boldsymbol{\varepsilon}_{tel} + \mathbf{S}_p\mathbf{q}_p + \mathbf{S}_s\mathbf{q}_s \tag{2.5}$$

The sensitivity matrix is partitioned into contributions from the primary and secondary mirrors. These partitions are still related to the global mode shapes, or rather to their projections on the primary and secondary mirror spaces.

Since a basis set generating a linear manifold is not unique, we still have the freedom to choose a basis set for each optical surface that may be different from the projection of the mode shapes.

The displacement of each point (node) on the optical surface, i.e. **q**, can be expressed as displacements in x, y, and z: (dc_x+δ**x**), (dc_y+δ**y**) and (δ**z**). The x and y directional averages for all nodes in the mirror dc_x, and dc_y, are separated out as the rigid body motion of the entire mirror, and called de-centers.

The circular shape of the mirror allows δ**z** to be described in a Zernike basis. Hence the mirror deformations can be written as Equation (2.6).

$$\boldsymbol{\delta z} = \begin{bmatrix} \delta z_1 \\ \vdots \\ \delta z_i \\ \vdots \\ \delta z_N \end{bmatrix} = \boldsymbol{\Gamma a} = \begin{bmatrix} \boldsymbol{\gamma}_0 & \boldsymbol{\gamma}_1 & \cdots & \boldsymbol{\gamma}_M \end{bmatrix} \begin{bmatrix} a_0 \\ a_1 \\ \vdots \\ a_M \end{bmatrix} = \begin{bmatrix} \gamma_{01} & \gamma_{11} & \cdots & \gamma_{M1} \\ \vdots & \vdots & \ddots & \vdots \\ \gamma_{0N} & \gamma_{1N} & \cdots & \gamma_{MN} \end{bmatrix} \begin{bmatrix} a_0 \\ a_1 \\ \vdots \\ a_M \end{bmatrix} \tag{2.6}$$

Here the Zernike functions $\boldsymbol{\gamma}_i$ are sampled on the same grid as the deformation. Practical considerations, like the requirement for uniform sampling to ensure the orthonormal property of the Zernike basis, may require re-sampling of the surface deformation.

If δ**x** and δ**y** are small enough compared to the x and y directional sampling interval, which is the node distance, they introduce only a slight irregularity in the sampling sequence. This irregularity will be neglected in expression (2.7), which leaves us with de-centers only. The deformation and displacement of the mirror can be expressed in terms of a new basis, which contains the de-centers dc_x and dc_y and the Zernike coefficients of the z directional surface deformation $[a_0, a_1, a_2 \ldots]^{\mathrm{T}}$.

$$\mathbf{q} = \begin{bmatrix} dc_x \\ dc_y \\ \delta z_1 \\ \vdots \\ dc_{xi} \\ dc_y \\ \delta z_i \\ \vdots \\ dc_x \\ dc_y \\ \delta z_N \end{bmatrix} = \begin{bmatrix} 1/\sqrt{N} & 0 & 0 & \cdots & 0 \\ 0 & 1/\sqrt{N} & 0 & \cdots & 0 \\ 0 & 0 & \gamma_{01} & \cdots & \gamma_{M1} \\ \vdots & \vdots & \vdots & \cdots & 0 \\ 1/\sqrt{N} & 0 & 0 & \cdots & 0 \\ 0 & 1/\sqrt{N} & 0 & \cdots & 0 \\ 0 & 0 & \gamma_{0i} & \cdots & \gamma_{Mi} \\ \vdots & \vdots & \vdots & \cdots & \vdots \\ 1/\sqrt{N} & 0 & 0 & \cdots & 0 \\ 0 & 1/\sqrt{N} & 0 & \cdots & 0 \\ 0 & 0 & \gamma_{0N} & \cdots & \gamma_{MN} \end{bmatrix} \begin{bmatrix} \sqrt{N} dc_x \\ \sqrt{N} dc_y \\ a_0 \\ \vdots \\ a_M \end{bmatrix} = \hat{\boldsymbol{\Gamma}} \hat{\mathbf{a}} \tag{2.7}$$

The original Zernike basis is orthonormal, therefore the extended basis set $\hat{\boldsymbol{\Gamma}}$ including de-centers can also be made orthonormal by the appropriate choice of the coefficients (*N* is the number of nodes involved).

By substituting Equations (2.7) back into Equation (2.5):

$$\boldsymbol{\varepsilon}_{exit} \approx \boldsymbol{\varepsilon}_{tel} + \mathbf{S}_p \hat{\boldsymbol{\Gamma}}_p \hat{\mathbf{a}}_p + \mathbf{S}_s \hat{\boldsymbol{\Gamma}}_s \hat{\mathbf{a}}_s \tag{2.8}$$

If the exit pupil OPD is also expanded on a Zernike basis ($\boldsymbol{\varepsilon}_{exit} = \boldsymbol{\Gamma}_{exit}\mathbf{a}_{exit}$), the Zernike coefficients $\mathbf{a}_{exit}$ are linear combinations of the extended Zernike coefficients $\hat{\mathbf{a}}_p$ and $\hat{\mathbf{a}}_s$ of the primary and secondary mirror deformation.

$$\begin{aligned} &\mathbf{a}_{exit} \approx \mathbf{a}_{tel} + \hat{\mathbf{S}}_p\hat{\mathbf{a}}_p + \hat{\mathbf{S}}_s\hat{\mathbf{a}}_s \qquad \text{where} \\ &\hat{\mathbf{S}}_p = \boldsymbol{\Gamma}_{exit}^{\mathrm{T}}\mathbf{S}_p\hat{\boldsymbol{\Gamma}}_p \\ &\hat{\mathbf{S}}_s = \boldsymbol{\Gamma}_{exit}^{\mathrm{T}}\mathbf{S}_s\hat{\boldsymbol{\Gamma}}_s \end{aligned} \tag{2.9}$$

Here $\mathbf{a}_{tel}$ is the Zernike expansion of the intrinsic aberrations of the un-deformed telescope for the given configuration and field angle.

By defining the output of the telescope optical system as the Zernike decomposition of the exit pupil OPD $\mathbf{a}_{exit}$, the optical output matrix of the telescope state space representation is significantly reduced in size. The size reduction is especially considerable, if the number of optically significant modes is limited, as it is usually the case in practice.

$$\mathbf{C} = \left(\hat{\mathbf{S}}_p\boldsymbol{\Gamma}_p^{\mathrm{T}}\boldsymbol{\Phi}_p + \hat{\mathbf{S}}_s\boldsymbol{\Gamma}_s^{\mathrm{T}}\boldsymbol{\Phi}_s\right)\begin{bmatrix}\mathbf{I} & \mathbf{0}\end{bmatrix} \tag{2.10}$$

3 CALCULATION OF THE SENSITIVITY MATRICES

The Zernike sensitivity matrices $\hat{\mathbf{S}}_p$ and $\hat{\mathbf{S}}_p$ can be generated directly by ray-tracing, similarly to the calculation of the full sensitivity matrix **S**. Let us assume that the Zernike coefficients of the OPD at the exit pupil can be expressed as second order polynomials in terms of the extended Zernike basis of the mirrors.

$$\mathbf{a}_{exit} = \mathbf{a}_{tel} + \hat{\mathbf{S}}_p\hat{\mathbf{a}}_p + \hat{\mathbf{S}}_s\hat{\mathbf{a}}_s + \hat{\mathbf{T}}_p\begin{bmatrix}\hat{a}_1^{\langle p\rangle 2}\\ \hat{a}_2^{\langle p\rangle 2}\\ \vdots\\ \hat{a}_{(M+2)}^{\langle p\rangle 2}\end{bmatrix} + \hat{\mathbf{T}}_s\begin{bmatrix}\hat{a}_1^{\langle s\rangle 2}\\ \hat{a}_2^{\langle s\rangle 2}\\ \vdots\\ \hat{a}_{(M+2)}^{\langle s\rangle 2}\end{bmatrix} + \hat{\mathbf{U}}\begin{bmatrix}\hat{a}_1^{\langle p\rangle}\hat{a}_1^{\langle s\rangle}\\ \hat{a}_2^{\langle p\rangle}\hat{a}_2^{\langle s\rangle}\\ \vdots\\ \hat{a}_{(M+2)}^{\langle p\rangle}\hat{a}_{(M+2)}^{\langle s\rangle}\end{bmatrix} \tag{3.1}$$

Our expectation is that for small deflections the first order terms in Equation (3.1) will dominate the second- and higher-order terms, so terms in $\hat{a}_k^{\langle i\rangle 2}$ and $\hat{a}_k^{\langle i\rangle}\hat{a}_{k'}^{\langle i'\rangle}$ can be truncated. If so, we have justified the linear model, in terms of the S matrices alone.

In order to calculate the elements of the coefficient matrices **S**, **T**, and **U,** mirror deformations and de-centers were introduced, term-by-term, into the ray-tracing model. To estimate the derivatives, for each mirror deformation Zernike term $a_k^{\langle i\rangle}$, 3 different deformation amplitudes (0 μm, 1 μm, and 2 μm) was applied. (Here *i* and *k* denote the optical surface and number of extended Zernike term, respectively.)

The OPD was evaluated over the exit pupil with a dense grid of rays, typically 100x100. The ray-traced OPD was then expressed as a linear combination of Zernike terms to very high accuracy (< 1nm residual). The corresponding Zernike coefficients, a_j were fitted with quadratic curves:

$$a_j = \alpha_j + \beta_{jk}^{\langle i\rangle}a_k^{\langle i\rangle} + \gamma_{jk}^{\langle i\rangle}\left(a_k^{\langle i\rangle}\right)^2 \tag{3.2}$$

The α coefficients go into $\mathbf{a}_{tel}$, the β coefficients into **S**, and the γ ones into **T**.

Obviously, the offset term $\mathbf{a}_{tel}$ is different for different field positions in the field of view of the telescope. This intrinsic telescope aberration is shown in Figure 3. The range of field angles (~10 arcmin) was chosen to significantly exceed the field of view of GSMT in Multiple-Conjugate Adaptive Optics operating mode (2 arcmin) [1]. Although in the case reported the field angle was applied in the y-z plane, it is fairly straightforward to extend the results for an arbitrary plane.

As is well known, the RMS wavefront aberration can be estimated as a weighted sum of the Zernike coefficient squares.

$$\sigma \simeq \sqrt{\sum_{j=1}^{N} w_j^2 a_j^2} \tag{3.3}$$

For the fringe Zernike used, non-unity weights, listed in the Appendix, are required. Figure 3 shows the total RMS wavefront aberration of the unperturbed telescope as a function of field angle.

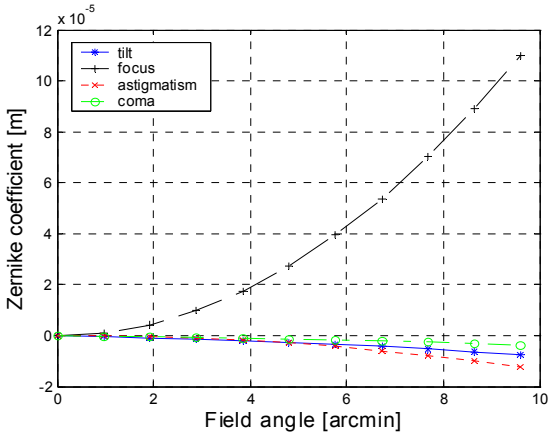

Figure 2 The Zernike coefficients (elements of $\mathbf{a}_{tel}$) for the unperturbed telescope estimated from the linear optical model ($\hat{\mathbf{a}}_p = \hat{\mathbf{a}}_s = \mathbf{0}$).

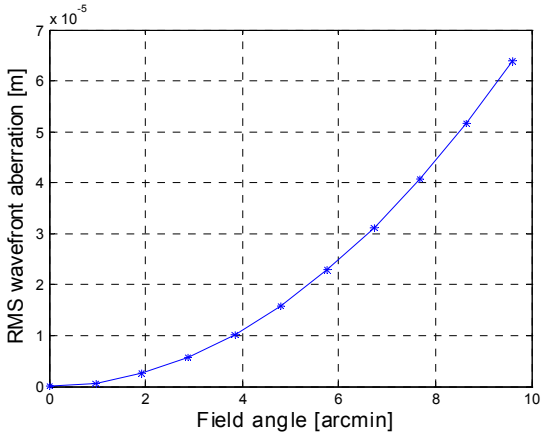

Figure 3 The RMS wavefront aberration of the unperturbed telescope estimated from the linear optical model ($\hat{\mathbf{a}}_p = \hat{\mathbf{a}}_s = \mathbf{0}$)

4 VALIDATION OF THE LINEAR MODEL

The structural deformations used for the validation of the linear model were derived from realistic conditions. An integrated model of the proposed Giant Segmented Mirror Telescope was developed in a Matlab environment [6], [9]. The structural model of the telescope, based on finite element analysis of the design was subjected to dynamic wind forces acting on the secondary mirror. The time-dependent vector wind velocity applied was real, measured wind velocity around the secondary mirror of Gemini South [10]. The mean wind speed was about 5 m/s. The drag forces were calculated by assuming a cylinder of 2 meters diameter and height. The telescope deformation was sampled for 30 seconds with 10 Hz sampling rate, resulting in 300 data sets. The primary mirror and the secondary mirror support legs were not exposed to wind to avoid the higher order deformations, which are well corrected by the edge sensor feedback loops.

A characteristic instant of primary mirror deformation is shown in Figure 4. The average secondary mirror de-center due to the wind load was about 14 μm, with average piston, tip and tilt Zernike coefficients of 29 μm, 0.06 μm, and 0.03 μm, respectively. For an on-axis beam, Figure 5 shows a characteristic output of the linear model as the average absolute Zernike coefficients of the exit pupil OPD.

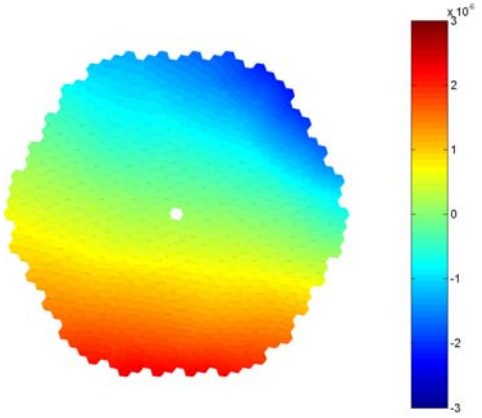

Figure 4 Characteristic deformation of the GSMT primary mirror in meter, under realistic wind load on the secondary mirror structure

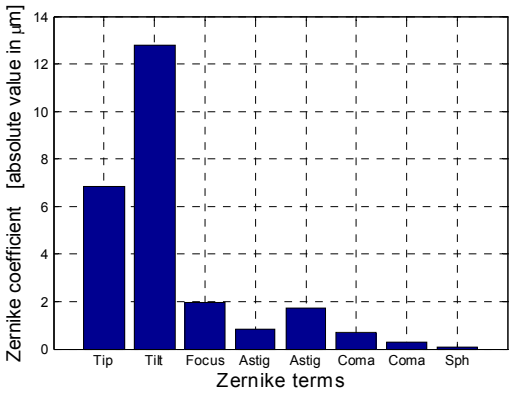

Figure 5 Average of the Zernike decomposition of the exit pupil OPD over 30 seconds, under realistic wind load on the secondary mirror structure

The validity of the linear model is verified by comparing the modeled OPD with the ray-traced OPD for the deformed telescope at each time instant. A dense (100 by 100) ray bundle was traced through the deformed telescope. The OPD was then expressed as a linear combination of 36 Zernike terms. The RMS residual wavefront error σ_{res} was calculated by subtracting the estimated Zernike coefficients a_j from the ray-traced coefficients $a_j^{\langle rt \rangle}$.

$$\sigma_{res} = \sqrt{\sum_{j=1}^{36} w_j^2 \left(a_j^{\langle rt \rangle} - a_j \right)^2} \tag{4.1}$$

Figure 6 shows the RMS residual wavefront errors and the ray-traced RMS wavefront aberrations for all 300 time-instants. Figure 7 shows the relative RMS residual wavefront error, which is referenced to the average ray-traced RMS wavefront aberration. The amplitude of the error is clearly negligible, less than 1 nm for the realistic deformation case.

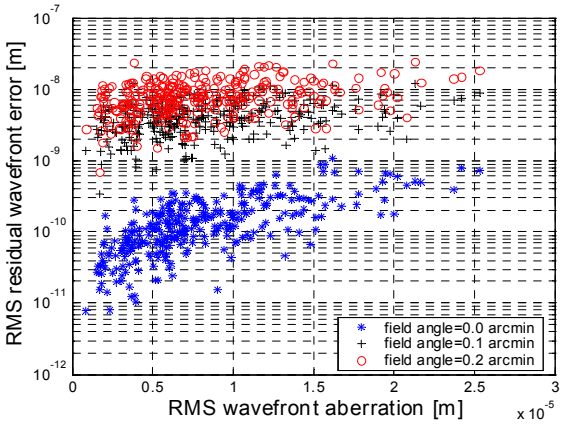

Figure 6 RMS residual wavefront errors σ_{res} versus RMS wavefront aberrations σ for close to on-axis beams

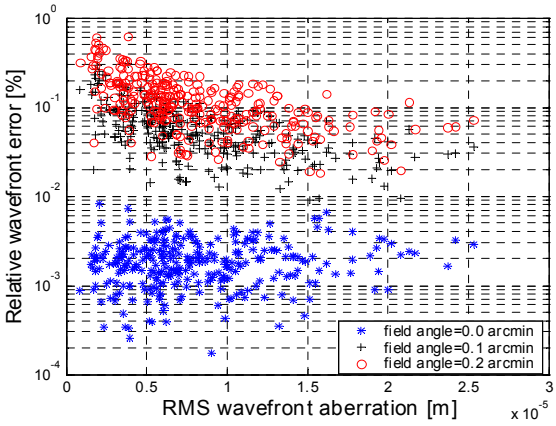

Figure 7 Relative RMS residual wavefront errors σ_{res} versus RMS wavefront aberrations σ_{rt} for close to on-axis beam

In order to explore the limits of the linear approximation, we investigated off-axis beams as a function of field angle (in the y-z plane), and disturbances amplified by a given scale factor. The scale factor was applied to all

deformations. The residual RMS wavefront errors averaged over the 300 samples are plotted as a function of the scale factor (Figure 8 and Figure 10) and the field angle (Figure 9 and Figure 11).

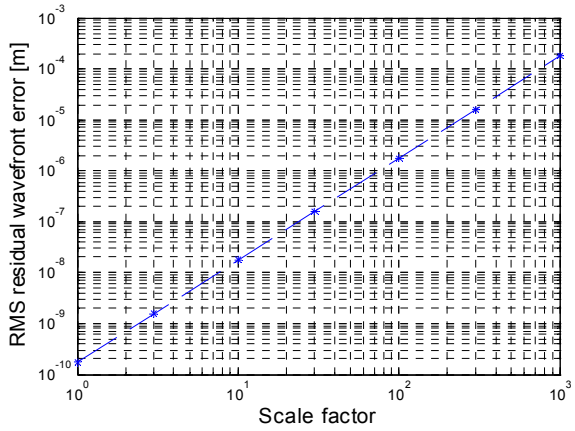

Figure 8 The average RMS residual wavefront error $\langle\sigma_{res}\rangle_{time}$ of the linear estimate as the function of deformation scale factor

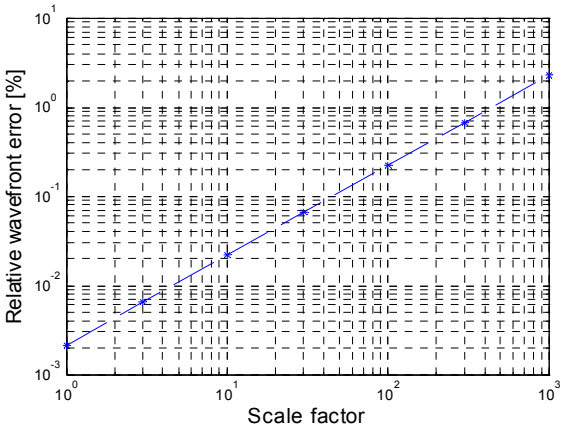

Figure 10 The average relative RMS residual wavefront error $\langle\sigma_{res}\rangle_{time}/\langle\sigma_{rt}\rangle_{time}$ of the linear estimate as the function of deformation scale factor

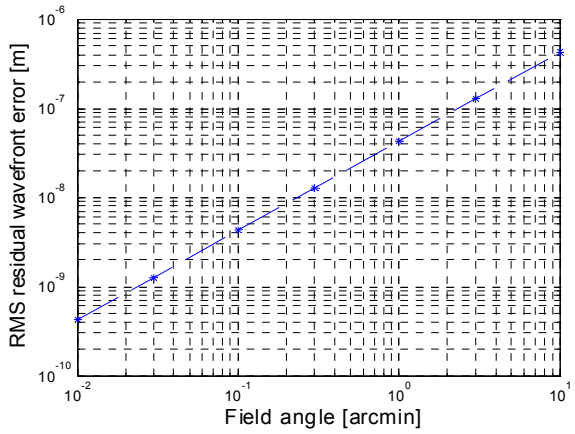

Figure 9 The average residual wavefront error $\langle\sigma_{res}\rangle_{time}$ of the linear estimate as the function of field angle

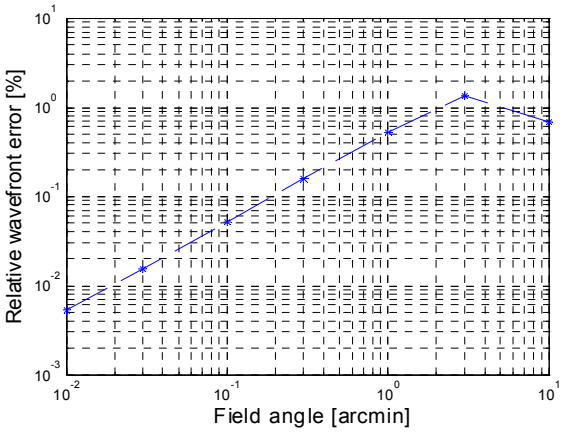

Figure 11 The average relative residual wavefront error $\langle\sigma_{res}\rangle_{time}/\langle\sigma_{rt}\rangle_{time}$ of the linear estimate as the function of field angle

5 CONCLUSIONS

Our calculations show that it is indeed practical to replace ray tracing with the suggested linear optical model in a significant class of situations characterized as follows.

- *The structural deformations, and consequently the optical surface displacements are adequately low order*. The model was validated with deformations containing no terms higher order than spherical aberration. In the case of the GSMT, the wind, gravitational and thermal disturbances are expected to fall into this category, because an edge-sensor based control loop maintains the continuity and higher order shape of the segmented primary mirror. For telescopes with a monolithic primary mirror, the stiffness of the glass and the mirror cell ensures the same result.

- *The amplitude of the deformations is limited.* For the GSMT, the error margin of estimating the RMS wavefront error due to telescope deformation was less than 1%, even with maximum deformations up to several mm. This limit is about 500 times higher than the average deformations due to realistic wind loads on the secondary support structure.

- *The field angle of the incoming beam is small enough*. For the current design of the GSMT we could keep the error margin of linear estimate below 100 nm (1%) for field angle up to 2 arcmin. This is 2 times higher than the expected telescope FOV in Multi-Conjugate Adaptive Optics (MCAO) observing mode.

There are several important advantages to the proposed Zernike based, linear model:

- The Zernike sensitivity matrices are significantly smaller than the full sensitivity matrix, which makes it easier to calculate and handle;

- The model provides an accurate and computationally efficient alternative to ray tracing to characterize the optical behavior of the telescope;

- The Zernike description provides a better understanding of deformation error propagation, because of the direct relationship established between the exit pupil OPD and mirror displacements and shapes;

- The simplicity of the model is well-matched to the most important operating mode of the large telescope: the behavior of the system close to the desired operating point;

ACKNOWLEDGEMENTS

The authors would like to thank Robert Upton of AURA New Initiatives Office for his valuable suggestions and comments. We are also grateful to Brent Ellerbroek and Myung Cho of AURA New Initiatives Office for their reviews and comments.

The New Initiatives Office is a partnership between two divisions of the Association of Universities for Research in Astronomy (AURA), Inc.: the National Optical Astronomy Observatory (NOAO) and the Gemini Observatory. NOAO is operated by AURA under cooperative agreement with the National Science Foundation (NSF). The Gemini Observatory is operated by AURA under a cooperative agreement with the NSF on behalf of the Gemini partnership: the National Science Foundation (United States), the Particle Physics and Astronomy Research Council (United Kingdom), the National Research Council (Canada), CONICYT (Chile), the Australian Research Council (Australia), CNPq (Brazil) and CONICET (Argentina)

REFERENCES

[1] *Enabling a Giant Segmented Mirror Telescope for the Astronomical Community*. http://www.aura-nio.noao.edu/book/index.html, AURA New Initiatives Office, 2002.

[2] W. K. Gawronski, *Dynamics and Control of Structures (A Modal Approach)*, (Springer-Verlag, New York, 1998).

[3] P. Avitabile, K. Weech, D. Smith, G. Gwaltney, and M. Sheehan, "Modal and Operating Characterization of an Optical Telescope" *Proceedings of the 19th International Modal Analysis Conference*, 2001.

[4] V. N. Mahajan, *Optical Imaging and Aberrations*, (SPIE, 1998).

[5] D. C. Redding and W. G. Breckenridge, "Optical Modeling for Dynamics and Control Analysis," *Journal of Guidance, Control, and Dynamics* **14**, 1021-1032 (1991).

[6] G. Z. Angeli, M. Cho, and M. S. Whorton, "Active optics and control architecture for a Giant Segmented Mirror Telescope," *Proceedings of SPIE* **4840**, 129-139 (2003).

[7] G. Chanan, J. E. Nelson, C. Ohara, and E. Sirko, "Design Issues for the Active Control System of the California Extremely Large Telescope (CELT)," *Proceedings of SPIE* **4004**, 363-372 (2000).

[8] D.G. MacMartin, G. Chanan, "Control of the California Extremely Large Telescope Primary Mirror", *Proceedings of the SPIE* **4840,** 69-80 (2002).

[9] G. Z. Angeli, A. Segurson, R. Upton, and B. Gregory, "Integrated modeling tools for large ground based optical telescopes," *Proceedings of SPIE* **5178** (2003).

[10] M. Cho, L. Stepp, and S. Kim, "Wind Buffeting Effects on the Gemini 8 m Primary Mirrors," *Proceedings of SPIE* **4444**, 302-314 (2001).

APPENDIX – ZERNIKE TERMS USED

The Zernike expansion used in this paper utilizes the so-called fringe or University of Arizona terms, which are normalized to unity maximum deformations rather than unity RMS deformations. This basis set is orthogonal, but not orthonormal. Wherever the mathematical deduction required the orthonormal property of the basis, the following weights were used. Nevertheless, the term numbering always corresponded to the fringe convention.

TERM NUMBER	TERM FUNCTION	WEIGHT
1	$\rho\cos\varphi$	$\frac{1}{\sqrt{4}}$
2	$\rho\sin\varphi$	$\frac{1}{\sqrt{4}}$
3	$2\rho^2-1$	$\frac{1}{\sqrt{3}}$
4	$\rho^2\cos 2\varphi$	$\frac{1}{\sqrt{6}}$
5	$\rho^2\sin 2\varphi$	$\frac{1}{\sqrt{6}}$
6	$\left(3\rho^3-2\rho\right)\cos\varphi$	$\frac{1}{\sqrt{8}}$
7	$\left(3\rho^3-2\rho\right)\sin\varphi$	$\frac{1}{\sqrt{8}}$
8	$6\rho^4-6\rho^2+1$	$\frac{1}{\sqrt{5}}$